Article:
Morse, Michael, Colin, Remy, Wilson, Laurence G. et al. (2016) The Aerotactic Response of Caulobacter crescentus. Biophysical Journal. pp. 2076-2084. ISSN: 0006-3495

https://doi.org/10.1016/j.bpj.2016.03.028

Aerotactic Response in *Caulobacter Crescentus*

Michael Morse[1], Remy Colin[2,3], Laurence G. Wilson[2,4], and Jay X. Tang[1]

[1]Department of Physics, Brown University, Providence, Rhode Island, USA

[2]Rowland Institute, Harvard University, Cambridge, Massachusetts, USA

[3]Max Planck Institute for Terrestrial Microbiology, Marburg, Germany

[4]Department of Physics, University of York, York, United Kingdom

Corresponding Author: Jay X. Tang, Brown University, 182 Hope St, Providence, RI, 02912

401-863-2292, E-mail: jay_tang@brown.edu

Many motile microorganisms are able to detect chemical gradients in their surroundings in order to bias their motion towards more favorable conditions. In this study, we observe the swimming patterns of *Caulobacter crescentus*, a uni-flagellated bacteria, in a linear oxygen gradient produced by a 3-channel microfluidic device. Using low magnification dark field microscopy, individual cells are tracked over a large field of view and their positions within the oxygen gradient are recorded over time. Motor switching events are identified so that swimming trajectories are deconstructed into a series of forward and backward swimming runs. Using this data, we show that *C. crescentus* displays aerotactic behavior by extending the average duration of forward swimming runs while moving up an oxygen gradient, resulting in directed motility towards oxygen sources. Additionally, motor switching response is sensitive to both the steepness of the gradient experienced and background oxygen levels, exhibiting a logarithmic response.

Introduction

Swimming motility plays an integral role in bacterial life as it allows cells to colonize new environments and acquire nutrients. For flagellated bacteria, motility is achieved by the rotation of helical flagella, which generate propulsive forces that are balanced by the viscous drag acting on a moving cell body. Each flagellum is powered by a motor at its base, embedded in the cell membrane. The motor can rotate in both the clockwise (CW) and counterclockwise (CCW) directions and periodically switches between the two states. Multi-flagellated bacteria such as *Escherichia coli*, which is often studied as a model swimmer, follow a two-step swimming process known as "run and tumble" (1). A run occurs when all flagella motors rotate in a single uniform direction (CCW for *E. coli*) so that the flagella form a rotating bundle that propels the cell forward through the surrounding medium. A tumble occurs when one or more motors switch their rotation direction so that the bundle unravels and the cell rapidly reorients. A cell's swimming trajectory is simply a series of relatively straight runs separated by large changes in direction due to tumbling. Uni-flagellated bacteria cannot tumble. Instead, a cell can either swim forward with the cell body leading or backward with the flagellum leading depending on the direction of motor rotation. Specifically for *Caulobacter crescentus,* CW and CCW motor rotations result in forward and backward swimming, respectively, due to the right handed helical structure of the flagellar filament (2). The cell can reorient itself, however, through a recently discovered process known as a flick (3). At the start of a forward run, the flexible flagellar hook buckles due to compressive force (4) and the cell body is rotated by a variable angle before the flagellum realigns with the central axis of the body and straight swimming is resumed. The probability a flick will occur depends on the swimming speed of the cell and the average turning angle depends on cell body size (5). As a result, a uni-flagellated cell's swimming trajectory is actually composed of three steps. The cell swims forward some distance; it swims straight backwards some distance; it then reorients itself through a flick before starting another forward run. The net displacement of the cell over each cycle depends on both the forward and backward run times.

The ability to direct their motion towards more favorable conditions through a well-known process called chemotaxis is critical to the survival of individual cells and the success of the species as a whole. In the presence of a spatial chemical gradient, a moving cell experiences a changing chemical concentration depending on its swimming trajectory. Through chemical signaling, the cell can alter the length of individual runs, resulting in directionally biased motility. If a cell senses increasing levels of an attractant, the motor(s) continue(s) to rotate in the same direction for a longer period of time, resulting in a longer run, both in terms of time and distance, before a tumble or flick reorients the cell. This behavior biases the cell's motion up gradients of chemical attractants. Chemical repellents have the opposite

effect and will cause the cell to stop the run sooner in order to reorient. Thus, the length of individual runs depends on the swimming direction relative to surrounding chemical gradients. Again, uni-flagellated swimmers have two different types of runs, forward and backward, either of which or both, can be potentially altered to achieve directed motility.

Many different experimental methods have been utilized to study chemotactic response in microbes, each of which has important advantages and disadvantages. A soft agar swimming assay, in which a petri dish filled with cell medium contained in a low percentage agar, displays the motility of a colony of microbes as they reproduce and spread (6). Introducing an attractant or repellent by mixing it into the agar will enhance or diminish this spread (7) as cells attempt to reach or avoid the surrounding region. This approach, however, is crude in spatial resolution and only the behavior of a large group of cells can be directly observed. In order to study chemotaxis at cellular scale, the local concentration of an attractant or repellent must change in a controlled manner over time while the behavior of the cell is observed. Chemicals of interest can be introduced into the cell medium either a quick pulse-like change (8, 9) or in continuous manner (10). Alternatively, a spatial gradient can be established in the cell medium so that the local concentration a cell senses varies due to its own swimming motion. The simplest method is to introduce the attractant or repellent through a pipette injection (11), creating a steep, radially directed gradient. Cells will swim towards and cluster around the pipette tip when an attractant is introduced. One difficulty with this design, however, is that the chemical gradient is highly variable both in magnitude and direction, especially near the source where most cells are clustered. In contrast, stable and uniform gradients can be established with the use of microfluidics. One simple design is a three parallel channel device, where the two outside channels act as a source and a sink. If the experimental chemical can diffuse between channels, a linear gradient is established across the width of the middle channel (12-15). One technical challenge is that the device must be made with a material that is permeable to the chemical of interest. More complex microfluidic devices have also been designed to mix multiple media and establish a uniform gradient (16). In addition to observing the swimming behavior of individual cells, techniques such as Forster Resonance Energy Transfer can be utilized to measure the internal response of the cells (17) and high throughput chemotaxis assays can provide population-scale time resolved chemotaxis measurements (18).

Aerotaxis, much like chemotaxis, enables cells to bias their motion based on local oxygen levels in order to reach ideal environmental conditions. A classic experimental demonstration is to suspend the cells in an open ended capillary tube and observe accumulation (19, 20). As the cells deplete the oxygen in their medium and new oxygen diffuses in from the end of the tube, an oxygen gradient is established. Cells then form a visible band as they cluster in the region with the optimal oxygen concentration.

Alternatively, air bubbles can be trapped in a sample, resulting in accumulation near the air-water interface (21). One limitation of these methods, much like the soft agar assay, is that only collective behavior of many cells is observed. Utilizing microfluidics techniques, similar experiments can be performed where the oxygen gradient can be controlled and well defined (22), allowing for the study of aerotactic response in a specific range of oxygen concentrations.

In this study, we utilize microfluidics to establish a linear oxygen gradient in order to characterize the aerotactic response of *C. crescentus* cells on the single cell level. To establish a constant linear oxygen gradient in the cells' swimming media, we utilize a three channel microfluidic device recently developed by the Stocker group (23, 24) that utilizes the oxygen permeability of PDMS (25). By observing many cells, we acquired a large data set consisting of forward and backward runs of variable length that traverse a wide range of local oxygen levels. We find that *C. crescentus* cells display an aerotactic response by prolonging the length of forward runs directed towards the oxygen source. Furthermore, the average run time varies roughly linearly with the ratio of the steepness of the gradient experienced by the cell and the background levels of oxygen present. This "logarithmic response" has previously been observed in the chemotactic response of other cells (13).

Materials and Methods

We made a microfluidic device with a three parallel channel design using PDMS. Using standard photolithography techniques, we produced a mold with a three parallel channel design (figure 1). PDMS was poured over the mold, hardened, and then peeled off. The resulting PDMS slab has three grooves indented on one face, corresponding to the channels from the mold. The middle channel is 1mm wide, and the side channels are each 600 μm wide. All three channels are 100 μm high. In between the channels is 200 μm of PDMS, which allows for the diffusion of oxygen between channels. The PDMS was adhered to a glass slide through oxygen plasma bonding (26) to prevent fluid from leaking out of the channels. Additionally, a glass coverslip was bound on top of the PDMS device to prevent the diffusion of ambient air into the channels from above. Holes were punched through the PDMS at both ends of each channel, providing an inlet and an outlet. The finished device was mounted on a microscope stage for observation. Two 5 mL glass syringes were filled with either pure nitrogen or atmospheric air with a partial pressure of oxygen (ppO_2) of 0 or 21 kPa, respectively. Polyethylene tubing was used to attach each syringe with a side channel inlet. Using a syringe pump (Harvard Apparatus), 50 μL/minute of each gas was flowed through the side channels in order to maintain a constant local ppO_2. For all experiments, the device was allowed to equilibrate for 30 minutes before observation in order to ensure that the gradient of oxygen across the middle channel was fully

established and steady.

We measured the oxygen levels in the device using an oxygen sensitive fluorescent dye, ruthenium-tris (4,7 diphenyl-1, 10-phenanthroline) dichloride ($Ru(dpp)_3CL_2$ or Rudpp) (Fluka). Oxygen quenches the fluorescence of the dye such that the observed intensity when the dye is at 21 kPa partial pressure of oxygen (ppO_2) is half of that as would be observed when the dye is in an oxygen depleted environment (27, 28). The Rudpp is not water soluble, but can be suspended by incorporating individual molecules in phospholipid micelles, which also renders the dye biologically inert (29). The concentrated dye was then loaded into the middle chamber of the microfluidic device. The entire width of the channel was imaged at 10x magnification, once the oxygen gradient was established. The dye was also imaged with atmospheric air flowing through both side channels so the entire middle channel was saturated at 21 kPa ppO_2 for the purpose of calibration. By comparing the fluorescence intensity from the two sets of images, the oxygen level can be calculated across the profile of the channel (see supplemental material). Moving from the oxygen source channel to the sink channel, the local oxygen concentration monotonically decreases. The gradient is approximately linear, which is expected given the nature of diffusion and the geometry of the device. The ppO_2 ranges from 6 to 16 kPa over the 1 mm width of the channel such that it rises at a constant rate of 0.01 kPa per micrometer.

Experiments in this report were performed using *Caulobacter crescentus* strain CB15 Δpilin, a mutant that lacks pili normally protruding from the cell body near the base of the flagellum, in order to reduce the number of cells adhered to the PDMS and glass surfaces of the microfluidic device. 20 mL of PYE (peptone yeast extract) growth medium (2 g/L Bacto peptone, 1 g/L Bacto yeast extract, 1.2 mM $MgSO_4$, and 0.5 mM $CaCl_2$) in a plastic petri dish was inoculated with the strain and incubated at 30°C on a shaker plate at 30 rpm for 24 hours (30). The depleted media along with suspended cells were emptied from the dish and replaced with fresh medium. Stalked cells attached to the bottom surface, which were not removed when the medium was replaced, were allowed to repopulate the new medium for an additional 24 hours during incubation. After this time, a thick carpet of stalked cells was present on the dish surface. The growth medium was replaced for the last time and, after several hours, enough free swimming cells had divided off so that there was sufficient density of cells for observation. Using a syringe, the middle channel of the microfluidic device was filled with the bacterial sample. Pieces of glass coverslip were then placed over both the inlet and outlet holes in order to plug the channel at both ends and prevent fluid flow. The central chamber was observed at 10x magnification using a dark field condenser so that only scattered light was collected by the objective and cells appeared as bright spots against a dark background. The microscope was focused on the top surface of the bacterial chamber (the PDMS side) in order to reduce the appearance of non-motile cells, which tended to sediment to the glass

slide at the bottom of the chamber. Additionally, this focal plane enabled us to differentiate between cells at the top and bottom of the channel, which are in and out of focus, respectively. Videos were taken of the middle channel at 20 frames per second with a large field of view that covered the entire 1mm width of the channel. These videos were cleaned digitally by removing background and enhancing contrast in order to isolate swimming cells.

Cells that were initially in the middle third of the chamber at the start of the video were manually tracked. The time and location of motor switching events, which can be identified by the cell's near instantaneous stopping and reversal in direction, were recorded (figure 2). In between every consecutive pair of switches is a run, either forward or backward and strictly alternating. We were able to differentiate between forward and backward runs due to the presence of the reorienting flick events, which occur at the start of some forward runs (figure 2B). When the cell started swimming backwards, in contrast, the swimming direction always reverses 180 degrees (figure 2A). The forward or backward runs can also be discerned by the handedness of circular swimming near the top or bottom surfaces. For example, when swimming near the top surface, backward runs follow a counterclockwise trajectory (figure 2D). Swapping either the swimming direction or the nearby surface also swaps the handedness. Backward runs tend to remain close to surfaces longer so that the curvature is more pronounced (30) whereas forward runs often leave the surface quickly so that the curvature is very localized and the average curvature over a run is close to zero with most reorientation due to rotational Brownian motion. Since forward and backward runs strictly alternate, the direction of every run could be determined using just one individual run's direction. We use additional flicks and curved swimming segments, however, as additional checks to insure high accuracy in differentiating run direction. For every forward or backward run, we determined the run time and the initial and final positions. Cells were followed for as long as possible, usually until the end of the recorded movie or their path intersected with another cell such that the two could not be reliably differentiated. Additionally, some cells (less than 5% of runs) left the field of view, due to a large net displacement over many runs. While this technique may fail to record some longer run times (which are already inherently rare), it reliably captures most runs and has no systematic bias dependent on swimming orientation that would skew results.

Combining the length of the runs with the knowledge of the oxygen concentration at all locations throughout the channel enables us to calculate the average rate of change in ppO_2 for each cell over time. Since the spatial oxygen gradient is stable over time, a cell's change in local oxygen level depends only on its displacement across the width of the channel due to swimming. Displacement, in turn, depends on swimming speed and direction. Cells swim at approximately 40 micrometers per second, though the speed of the fastest and slowest cells can vary by over a factor of two. The low magnification

and spatial resolution of this apparatus limits the precision of measurements of instantaneous swimming speed, however, previous experiments have shown that both swimming speed and motor rotation rates remain constant for a single cell over multiple runs (31, 32). The directions of individual runs are roughly isotropically distributed. Cells swimming directly towards the oxygen source experience the steepest increase in oxygen level while the opposite is true for cells swimming directly towards the oxygen sink. As a result, while the spatial oxygen gradient is constant in our experiment, the observed runs cover a range of +/- 0.5 kPa ppO_2 per second.

Results

As an initial test for aerotactic response, we separate our data into runs directed up the oxygen gradient (swimming towards the air channel) and down the oxygen gradient (swimming towards the nitrogen channel). Specifically, we separate runs that result in a net increase or decrease in oxygen level based on the run's start and end position in the channel. For each condition, we plot the distribution of run times and calculate the average run time for both forward and backward runs in order to check for aerotactic effects (figure 3). The distribution was created by binning the run times in 0.2 second intervals. All distributions have the same rough shape, with a peak slightly under one second representing the most probable run times and a long tail decaying to zero at longer times. The distributions can be approximated as inverse Gaussians which are provided as fit lines to highlight the underlying trend in each distribution.

$$P(t) = \sqrt{\frac{\lambda}{2\pi t^3}} \exp\left(\frac{-\lambda(t-\mu^2)}{2\mu^2 t} \right)$$

P(t) is the probability density of run time given a mean value μ and a shape parameter λ. Similar distributions of run time have previously been observed under non-chemotactic conditions for both *C. Crescentus (32)* and *Vibrio Alginolyticus (3)*, another uni-flagellated bacterium. While run time for non-chemotactic cells can be fit exactly with an inverse Gaussian, here individual cells obey slightly different statistics due to the heterogeneous environment. Backwards swimming cells, both up and down the oxygen gradient, have short average run times of approximately 1.3 seconds. The distribution is also sharply peaked such that over 80% of runs last less than 2 seconds. In contrast, the average length of forward runs is significantly longer, with more runs lasting several seconds. Most notably, we find a significant difference in forward run time for cells moving up versus down the oxygen gradient. Cells experiencing increasing and decreasing oxygen levels have average run times of 2.2 and 1.8 seconds,

respectively. The aerotactic behavior can also be seen in the run time distribution for cells swimming towards the oxygen source, displaying fewer cells in the short time peak and more in the long time tail. We also plot our run time data as a cumulative distribution, which shows the probability that a run will end before a given time. Cumulative distributions also do not require binning and display less noise, making visual comparisons between conditions easier. It is clear that a motor is more likely to switch at an earlier time when the cell senses decreasing oxygen levels. Backwards runs, in contrast, were uniformly short regardless of swimming direction. As such, all further analysis is focused solely on forward runs. As a control, we also repeated our measurements with both channels of our device containing atmospheric air such that the bacterial chamber is saturated at 21 kPa ppO_2. The results of this control experiment confirm that average run length is not correlated with swimming orientation in a medium without any spatial oxygen gradient.

A cell's sensitivity to changing oxygen levels may also depend on background levels of oxygen. For example, an increase of 1 kPa partial pressure of oxygen may elicit a different response in cells that are initially at a high or low oxygen level. When swimming in a steep gradient, the local oxygen level for a given cell is rapidly changing. Thus, every cell observed has a slightly different effective background oxygen level based on its current location and its previous positions in the gradient. To test for background dependent effects, we further separate runs based on the cell's oxygen level at the start of the run. This initial ppO2 also serves as an unbiased estimate of a cell's past oxygen levels (see supplemental material). In previous studies on other cells, long timescale adaptation has been observed over the timescale of minutes (33). In this study, however, we instead focus on the fast time scale response of *Caulobacter*, as the steep gradient and the cell's rapidly changing local oxygen level would severely inhibit long time scale adaptation. Additionally, we do not observe significant run time dependence between consecutive runs (see supplemental material). Since the middle of the channel is at 11 kPa ppO_2, we distinguish between runs that begin above or below this value. We once again compute the average run time and cumulative distribution of run times for cells moving both up and down the oxygen gradient (figure 4). For cells that begin a run above 11 kPa ppO_2, the increase in run time for cells moving up the oxygen gradient is no longer statistically significant. For cells starting runs below 11 kPa ppO_2, however, the increase in run time is greatly augmented. The cumulative distributions for cells in the high oxygen region appear very similar, whereas there is a distinct shift to longer run time for cells initially at low oxygen levels that swim towards the oxygen source.

The rate at which a cell's local oxygen level rises or falls may also impact run time. We quantify the steepness of the oxygen gradient experienced by a cell over each run to test for this effect. Simply dividing the change in ppO_2 over a run by the run time gives the absolute rate of change in ppO_2. This

value, however, fails to take into account background oxygen level, which we have just demonstrated affects run time. Thus, for each run, we calculated the relative rate of change in oxygen, which is the absolute rate of change in ppO_2 divided by the ppO_2 at the start of the run.

$$\text{Relative Rate of Change} = \frac{(\Delta ppO_2)/(\Delta t)}{ppO_2(initial)}$$

For example, an increase of 0.1 kPa in a background of 1 kPa over 2 seconds is the same relative increase, 5% per second, as an increase of 1 kPa in a background of 10 kPa over 2 seconds. The runs in our data set have relative rates of change between plus or minus 8% per second. We separate runs into 4 bins of equal width based on relative rate of change and again calculate average run time and run time cumulative distribution (figure 5). The four bins correspond to quickly decreasing, slowly decreasing, slowly increasing, and quickly increasing oxygen levels. We also calculate the average run time as a function of relative rate of oxygen increase using a moving bin of the same size (+/- 2% per second). For comparison, runs with a rate of change of less than 1% per second, last an average of 1.85 seconds. Average run time is positively correlated with relative rate of change and monotonically increases as the rate increases. Additionally, the increase in run time for cells experiencing increases in oxygen level is significantly larger than the decrease in run time for cells experiencing decreases in oxygen level. The cumulative distributions confirm this effect by displaying a larger shift in run time between slow and quick oxygen increases than between slow and quick oxygen decreases

Discussion

The mechanics of how the flagellar motor switches between CW and CCW rotations are tightly coupled to the sensory regulation of the flagellar motor. Most important for directed motility is the ability of the cell to change the frequency of switching between the two rotational states. It is well established that CheY-P, the phosphorylated form of a signaling protein Che-Y, promotes CW rotation of the motor (34). That is, higher intracellular levels of CheY-P result in a larger CW bias, the fraction of time the motor is rotating in the CW direction. For example, CW bias values of 0, 1, and 0.5 indicate the motor is always rotating CCW, always rotating CW, and rotating in both directions for equal amounts of time, respectively. For *Caulobacter*, CW motor rotation results in forward swimming due to the right handed helicity of its flagellum (2). Thus, a chemical which induces an increased CW bias in *Caulobacter* acts as an attractant, as forward runs become much longer than backward runs, increasing net displacement of the cell towards the source over each complete motor switching cycle.

Our results indicate that cells experiencing increasing oxygen levels increase their CW bias. Additionally, the degree to which CW bias is increased depends on both background levels of oxygen and the steepness of the gradient experienced. This behavior has been previously shown in the chemotactic response of multiple other bacterial species and is known as logarithmic sensing (13). Specifically, the response of the cell is not proportional to the gradient experienced, but rather the gradient experienced relative to the background concentration. In figure 5C, we observe the change in run time increases roughly linearly with respect to the ratio of the rate of change in oxygen concentration and the cell's initial oxygen concentration before the start of the run. Thus, our finding confirms the logarithmic sensing.

Logarithmic response to oxygen gradients has ecological implications for bacterial life. The ability to respond more sensitively to even shallow gradients when cells reside in an oxygen depleted environment is beneficial to their survival. Conversely, when at sufficiently higher oxygen levels, the cells would not require oxygen seeking behavior as direly. Additionally, while the cells display logarithmic response to both increases and decreases in oxygen, increases result in a larger change in average run time than decreases of equal magnitude. A similar behavior has been observed in *E. coli* where the cell prolongs runs substantially while swimming up chemical gradients and increases tumbling frequency only slightly when swimming down gradients (35). An asymmetrical response to attractant will have a substantial impact on the swimming patterns of a cell and should be taken into account when modeling cell motility. There are two possible origins of this asymmetry. Most directly, cell signaling may modulate intracellular levels of CheY-P by different degrees dependent on increasing or decreasing attractant levels. Alternatively, the flagellar motor switching mechanism itself may respond to variable CheY-P levels in a nonlinear manner. This would be consistent with measurements of CW bias in cells, which is a sigmoidal function of CheY-P concentration in *E. Coli* (34). Our recent CheY-P binding dependent model of motor switching in *Caulobacter crescentus* also shows this relationship (32).

While aerotaxis superficially resembles chemotaxis in that a cell biases its motion in response to changing chemical concentrations, there are important distinctions. Most importantly, aerotaxis is a metabolism dependent process while chemical signaling in response to attractants and repellents is not (36). Two different modes of response have been observed in cells responding to changing oxygen levels. Some studies on multi-flagellated bacteria have observed that increasing or decreasing oxygen levels can alter the tumbling (or switching) frequency of cells (20, 37). This is achieved by altering the CW bias of the cell, much like chemotactic response. Other studies have observed that the proton motive force that powers the flagellar motor is altered by changing oxygen concentration (19, 38). This leads to

a different model of directed motility, in which the cells change their swimming speed in order to bias their motion. By swimming faster when approaching favorable conditions and slower when leaving, a cell can direct its motility without altering run time length. Alternatively, by swimming at a slower speed after reaching favorable conditions, cells can increase their dwell time in this region, resulting in population accumulation (39). We found no evidence, however, that the swimming speeds the cells in our experiment depend on either the local oxygen level or its change over time (see supplemental material). Thus, our results more closely resemble the first scenario in which cells change their tumbling or switching frequency in order to direct motility. By altering the CW bias of its flagellar motor, *Caulobacter* changes the ratio of forward to backward swimming durations in order to achieve directed motility.

While the average durations of CW and CCW motor rotation are often used as a quantitative measure of motor function, the distribution of motor run times is not trivial. If switching between rotation directions was controlled by a rate constant though Poisson statistics, the distribution of run times would simply be an exponential decay. Our results, however, show a markedly different, peaked distribution. Of particular note, we see very few runs near zero seconds, which should occur most frequently for Poisson switching. Interestingly, both exponential and peaked distributions have been observed for *E. coli* motors under different experimental conditions (40-46). While we have previously observed a similar distribution for *Caulobacter* under non-chemotactic conditions (32), we can now observe how this distribution changes as the average run length is increased. For Poisson switching, runs can be lengthened by simply decreasing the switching rate, which would result in a more gradual exponential decay in the distribution. In our results, we see the same basic shape in all distributions with the peak at the same value. The average run time can be shifted, however, due to a longer and fatter tail at long run times at the expense of run times in the peak region. This feature may provide key insights as to how directed motility for uni-flagellated swimmers may be controlled in a different manner than multi-flagellated swimmers.

The device and methods used in this study also provide some unique insights on results from previous works. In many aerotaxis experiments, oxygen is introduced into the system via air bubbles or pockets. Accumulation near these oxygen sources could be mistaken as proof of aerotaxis due to the following complicating factors. The air-water interface exerts physical forces on cells that alter swimming behavior. Most notably, high surface tension acts as a solid barrier on incoming cells, resulting in surface accumulation (47-49). Furthermore, depending on the chemical composition of the surface, the lateral movement of cells can be altered in unexpected ways. In our experiments, we avoid such complications by focusing only on the region where the cells do not encounter surfaces while

moving up and down the oxygen gradient. Additionally, many experiments rely on large scale phenomena, such as accumulation, in order to demonstrate aerotactic behavior. This can be difficult to achieve using *Caulobacter* for two reasons. Caulobacter has a two-stage life cycle, where swimming cells shed their flagella before reproducing. Thus, established colonies consist mainly of immotile cells, rendering experiments based on accumulation irrelevant. Also, *Caulobacter* swarmer cells are fast swimmers, traveling on average over 50 microns per second. The fast swimming speed, combined with the random swimming orientation of each run and the constraints of the chamber, greatly diminishes accumulation.

Concluding Remarks

Our data show that *Caulobacter crescentus* swarmer cells clearly exhibit aerotactic behavior by altering the length of forward swimming runs in response to oxygen gradients. Additionally, this effect is most pronounced when the cell experiences large relative increases in local oxygen levels. This result is consistent with the logarithmic response exhibited by a variety of chemotactic cells. The manner in which run times are increased is not a trivial multiplicative factor. Instead, all run time distributions have the same general form with a peak at the same value. The average run time is dictated by the relative sizes of the peak and the decaying tail. Uni-flagellated bacteria not only follow a different swimming pattern than multi-flagellated bacteria, their bias in motion is also controlled in a distinct manner. Observation of other uni-flagellated swimmers has also seen asymmetric response for the two different flagellar rotation directions (50). Together, these new findings point to how rather differently monotrichous and peritrichous bacteria have evolved in their response to environmental cues.

Author Contributions

MM, RC, LGW, and JXT designed research. MM and RC performed experiments. MM analyzed data. MM and JXT wrote the manuscript.

Acknowledgments

We acknowledge support of this work by NSF Grants PHY 1058375 and CBET 1438033. We thank Professors Y. Brun (Indiana University) for providing the bacterial strain used in the study, R. Stocker (MIT) for providing the photo mask used to produce the microfluidic device, and H. Salman (University of Pittsburgh) for providing the protocol for producing Ru-dpp micelles.

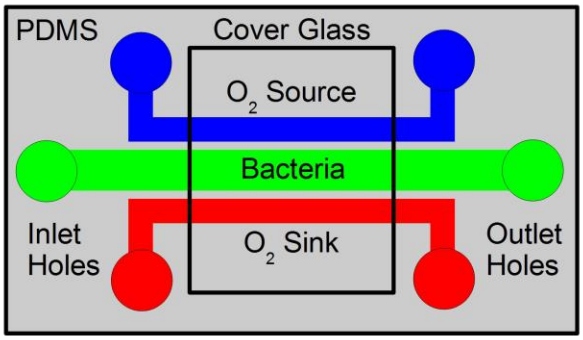

Fig. 1. (Top) Diagram of the microfluidic device used for aerotaxis measurements. The width of the channels and the spacing between them are drawn to scale. The middle chamber, which holds the bacterial sample, is 1mm in width and is plugged at both ends with glass coverslip pieces during observation. The side channels are 600 μm in width and are constantly flowed through with air or nitrogen at a rate of 50 μL/min. The PDMS barrier between the channels is 200 μm in width, and the height of all channels is 100 μm. The glass slide and coverslip above and below the device prevent the ambient air from diffusing into the device so that the main sources of oxygen and nitrogen are the side channels. (Bottom) Partial pressure of oxygen measured across the width of the channel using fluorescent dye. Each blue dot is a calculated oxygen concentration for a row of pixels in the fluorescence image and the red line is a linear best fit. Oxygen levels range from 6 to 16 kPa such that the partial pressure of oxygen increases at a rate of 0.01 kPa per μm moving across the width of the channel.

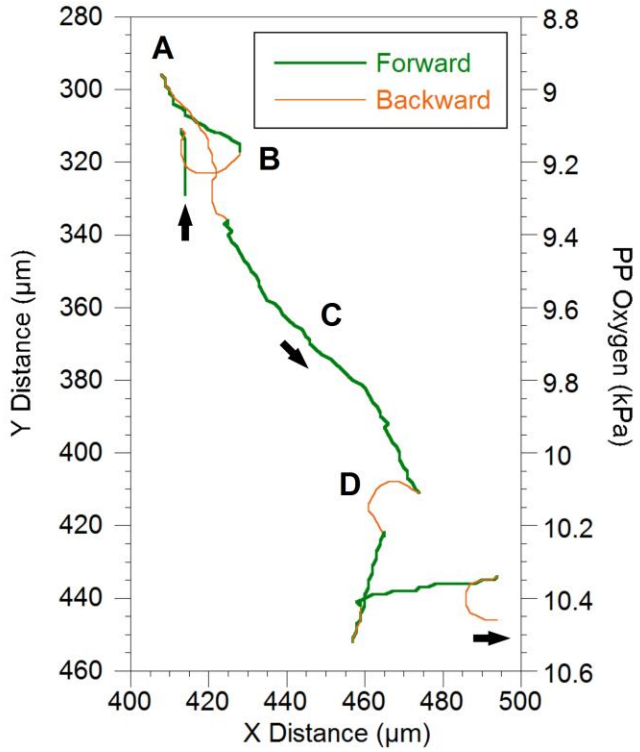

Fig. 2. Representative trajectory of a cell swimming in the microfluidic device. In this perspective, the air channel is located below the graph and runs along the X coordinate direction, such that the local oxygen partial pressure increases as the cell moves down the image. Forward and backward swimming segments are marked as green and orange, respectively, and arrows indicate swimming direction. Features to note include: (A) an exact reversal in swimming direction at the start of a backward swimming, (B) a variable angle turn at the start of a forward swimming, (C) a prolonged run as the cell moves up the oxygen gradient, and (D) CCW circular backwards swimming trajectory near the PDMS surface. Each cell swims at a near constant speed, around 50 µm/s, so that the total displacement over a run is proportional to the run time.

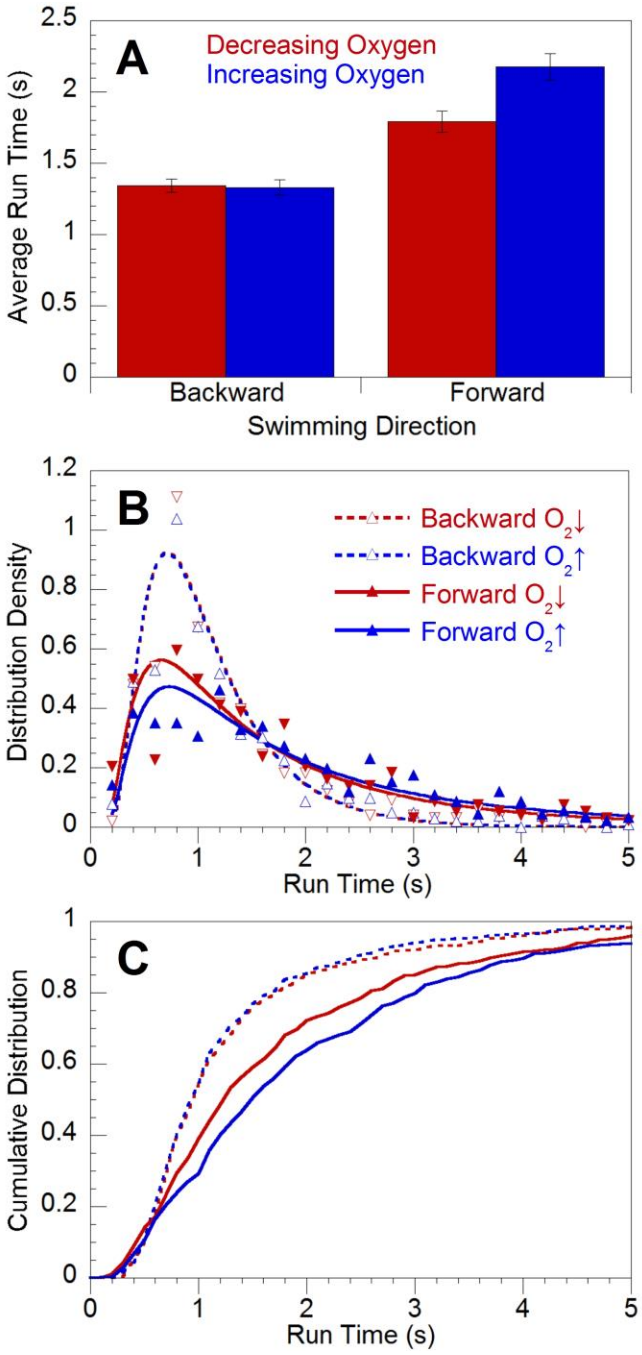

Fig. 3. Measurements of run time for cells moving in an oxygen gradient. (A) A bar plot shows the average forward or backward run time for cells swimming either up or down the oxygen gradient. Error bar shown is standard error of the mean. (B) Distributions of run times are plotted as triangles using bins of size 0.2 seconds. Each fit line follows an inverse Gaussian distribution with the mean parameter equal to the average run time for that condition. Each distribution peaks around 1 second and decays

exponentially at longer times. (C) Cumulative distributions for the same data show a distinct shift to longer run time both for forward swimming as compared to backward swimming, and forward swimming up the oxygen gradient as compared to forward swimming down the gradient. The integrated space above the curve is equal to the average run time. A total of 1026 backward runs and 942 forward runs were observed.

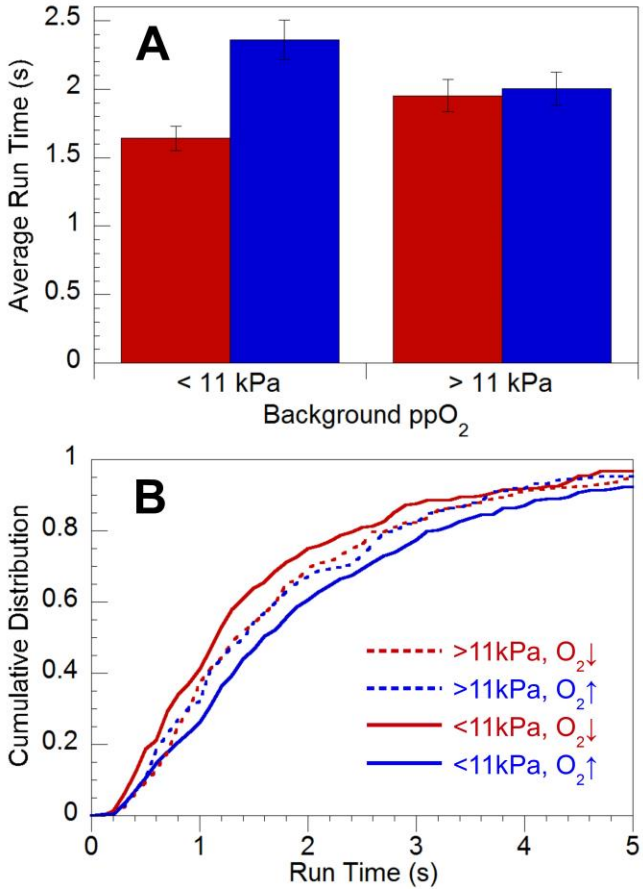

Fig. 4. Average run times (A) and cumulative distributions of run times (B) for forward swimming cells moving up or down the oxygen gradient and in high or low background oxygen environments (above or below 11 kPa partial pressure of oxygen, respectively). In low background oxygen environments, the difference in run time between swimming up or down the oxygen gradient is augmented. In high background oxygen environments runs up or down the oxygen gradient are similar in length.

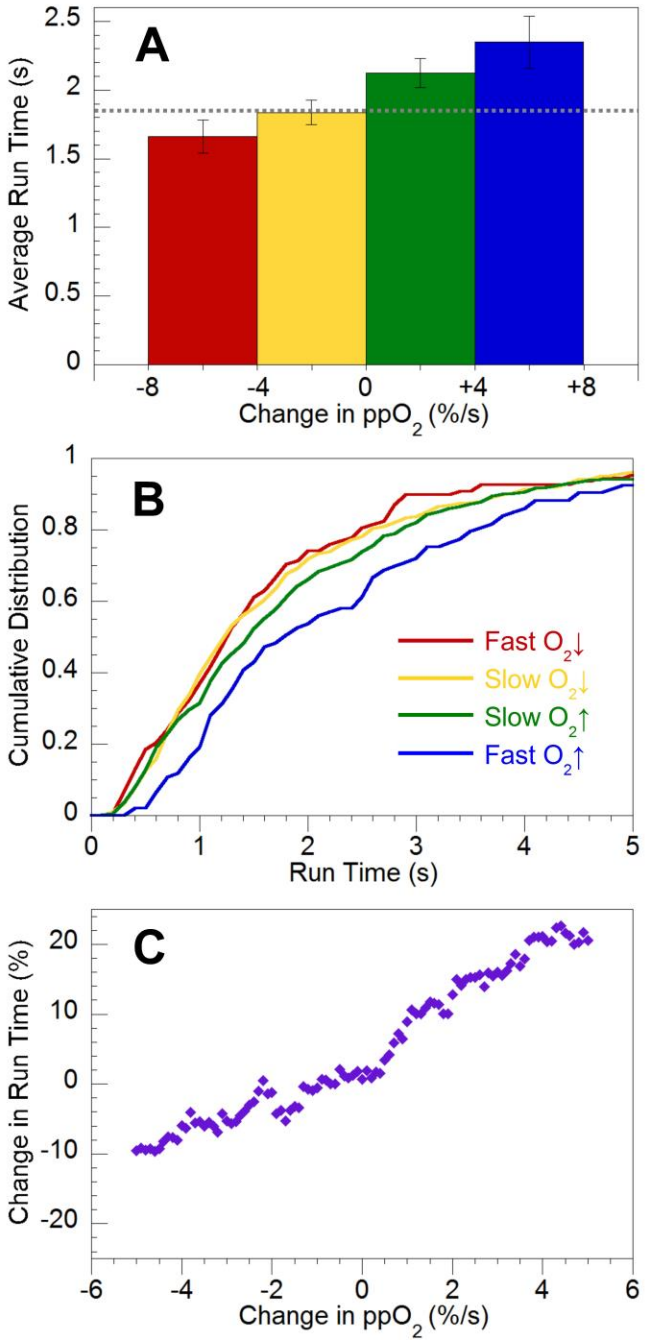

Fig. 5. Average run times (A) and cumulative distributions of run times (B) for forward swimming cells based on the relative rate of change in local oxygen concentration. Note a consistent color scheme is applied to A and B. The dashed gray line in (A) marks the average run time for cells that experience negligible changes in oxygen level. Run length increases as the relative rate of change of oxygen increases. The average run time as a function of relative rate of change is also plotted using a moving

bin of size +/- 2 percent per second (C). The increase in run length for cells moving up the oxygen gradient is larger than the decrease in run length for cells moving down the oxygen gradient.

References

1. Berg, H. C. 2008. E. coli in Motion. Springer Science & Business Media.
2. Koyasu, S., and Y. Shirakihara. 1984. Caulobacter crescentus flagellar filament has a right-handed helical form. Journal of molecular biology 173:125-130.
3. Xie, L., T. Altindal, S. Chattopadhyay, and X.-L. Wu. 2011. Bacterial flagellum as a propeller and as a rudder for efficient chemotaxis. Proceedings of the National Academy of Sciences 108:2246-2251.
4. Son, K., J. S. Guasto, and R. Stocker. 2013. Bacteria can exploit a flagellar buckling instability to change direction. Nature physics 9:494-498.
5. Taute, K., S. Gude, S. Tans, and T. Shimizu. 2015. High-throughput 3D tracking of bacteria on a standard phase contrast microscope. Nature communications 6.
6. Wolfe, A. J., and H. C. Berg. 1989. Migration of bacteria in semisolid agar. Proceedings of the National Academy of Sciences 86:6973-6977.
7. Tso, W.-W., and J. Adler. 1974. Negative chemotaxis in Escherichia coli. Journal of bacteriology 118:560-576.
8. Macnab, R. M., and D. Koshland. 1972. The gradient-sensing mechanism in bacterial chemotaxis. Proceedings of the National Academy of Sciences 69:2509-2512.
9. Block, S. M., J. E. Segall, and H. C. Berg. 1982. Impulse responses in bacterial chemotaxis. Cell 31:215-226.
10. Segall, J. E., S. M. Block, and H. C. Berg. 1986. Temporal comparisons in bacterial chemotaxis. Proceedings of the National Academy of Sciences 83:8987-8991.
11. Altindal, T., S. Chattopadhyay, and X.-L. Wu. 2011. Bacterial chemotaxis in an optical trap. PLOS one 6:e18231.
12. Diao, J., L. Young, S. Kim, E. A. Fogarty, S. M. Heilman, P. Zhou, M. L. Shuler, M. Wu, and M. P. DeLisa. 2006. A three-channel microfluidic device for generating static linear gradients and its application to the quantitative analysis of bacterial chemotaxis. Lab on a Chip 6:381-388.
13. Kalinin, Y. V., L. Jiang, Y. Tu, and M. Wu. 2009. Logarithmic sensing in Escherichia coli bacterial chemotaxis. Biophysical journal 96:2439-2448.
14. Kovarik, M. L., P. J. Brown, D. T. Kysela, C. Berne, A. C. Kinsella, Y. V. Brun, and S. C. Jacobson. 2010. Microchannel-nanopore device for bacterial chemotaxis assays. Analytical chemistry 82:9357-9364.
15. Ahmed, T., T. S. Shimizu, and R. Stocker. 2010. Microfluidics for bacterial chemotaxis. Integrative Biology 2:604-629.
16. Englert, D. L., M. D. Manson, and A. Jayaraman. 2009. Flow-based microfluidic device for quantifying bacterial chemotaxis in stable, competing gradients. Applied and environmental microbiology 75:4557-4564.
17. Sourjik, V., and H. C. Berg. 2002. Receptor sensitivity in bacterial chemotaxis. Proceedings of the National Academy of Sciences 99:123-127.
18. Colin, R., R. Zhang, and L. G. Wilson. 2014. Fast, high-throughput measurement of collective behaviour in a bacterial population. Journal of The Royal Society Interface 11:20140486.
19. Zhulin, I. B., V. A. Bespalov, M. S. Johnson, and B. L. Taylor. 1996. Oxygen taxis and proton motive force in Azospirillum brasilense. Journal of bacteriology 178:5199-5204.
20. Laszlo, D. J., and B. L. Taylor. 1981. Aerotaxis in Salmonella typhimurium: role of electron transport. Journal of bacteriology 145:990-1001.
21. Bibikov, S. I., R. Biran, K. E. Rudd, and J. S. Parkinson. 1997. A signal transducer for aerotaxis in Escherichia coli. Journal of bacteriology 179:4075-4079.
22. Adler, M., M. Erickstad, E. Gutierrez, and A. Groisman. 2012. Studies of bacterial aerotaxis in a microfluidic device. Lab on a Chip 12:4835-4847.
23. Yawata, Y., O. X. Cordero, F. Menolascina, J.-H. Hehemann, M. F. Polz, and R. Stocker. 2014.

Competition–dispersal tradeoff ecologically differentiates recently speciated marine bacterioplankton populations. Proceedings of the National Academy of Sciences 111:5622-5627.
24. Rusconi, R., J. S. Guasto, and R. Stocker. 2014. Bacterial transport suppressed by fluid shear. Nature physics 10:212-217.
25. Gray, J. M., D. S. Karow, H. Lu, A. J. Chang, J. S. Chang, R. E. Ellis, M. A. Marletta, and C. I. Bargmann. 2004. Oxygen sensation and social feeding mediated by a C. elegans guanylate cyclase homologue. Nature 430:317-322.
26. Ginn, B. T., and O. Steinbock. 2003. Polymer surface modification using microwave-oven-generated plasma. Langmuir 19:8117-8118.
27. Bacon, J., and J. Demas. 1987. Determination of oxygen concentrations by luminescence quenching of a polymer-immobilized transition-metal complex. Analytical chemistry 59:2780-2785.
28. Klimant, I., and O. S. Wolfbeis. 1995. Oxygen-sensitive luminescent materials based on silicone-soluble ruthenium diimine complexes. Analytical chemistry 67:3160-3166.
29. Douarche, C., A. Buguin, H. Salman, and A. Libchaber. 2009. E. Coli and oxygen: a motility transition. Physical review letters 102:198101.
30. Li, G., L.-K. Tam, and J. X. Tang. 2008. Amplified effect of Brownian motion in bacterial near-surface swimming. Proceedings of the National Academy of Sciences 105:18355-18359.
31. Liu, B., M. Gulino, M. Morse, J. X. Tang, T. R. Powers, and K. S. Breuer. 2014. Helical motion of the cell body enhances Caulobacter crescentus motility. Proceedings of the National Academy of Sciences 111:11252-11256.
32. Morse, M., J. Bell, G. Li, and J. X. Tang. 2015. Flagellar Motor Switching in Caulobacter Crescentus Obeys First Passage Time Statistics. Physical review letters 115:198103.
33. Lazova, M. D., T. Ahmed, D. Bellomo, R. Stocker, and T. S. Shimizu. 2011. Response rescaling in bacterial chemotaxis. Proceedings of the National Academy of Sciences 108:13870-13875.
34. Cluzel, P., M. Surette, and S. Leibler. 2000. An ultrasensitive bacterial motor revealed by monitoring signaling proteins in single cells. Science 287:1652-1655.
35. Berg, H. C., and D. A. Brown. 1972. Chemotaxis in Escherichia coli analysed by three-dimensional tracking. Nature 239:500-504.
36. Taylor, B. L., I. B. Zhulin, and M. S. Johnson. 1999. Aerotaxis and other energy-sensing behavior in bacteria. Annual Reviews in Microbiology 53:103-128.
37. Repik, A., A. Rebbapragada, M. S. Johnson, J. Ö. Haznedar, I. B. Zhulin, and B. L. Taylor. 2000. PAS domain residues involved in signal transduction by the Aer redox sensor of Escherichia coli. Molecular microbiology 36:806-816.
38. Shioi, J., and B. L. Taylor. 1984. Oxygen taxis and proton motive force in Salmonella typhimurium. Journal of Biological Chemistry 259:10983-10988.
39. Schnitzer, M. J. 1993. Theory of continuum random walks and application to chemotaxis. Physical Review E 48:2553.
40. Block, S. M., J. E. Segall, and H. C. Berg. 1983. Adaptation kinetics in bacterial chemotaxis. Journal of bacteriology 154:312-323.
41. Fahrner, K. A., W. S. Ryu, and H. C. Berg. 2003. Biomechanics: bacterial flagellar switching under load. Nature 423:938-938.
42. Korobkova, E., T. Emonet, J. M. Vilar, T. S. Shimizu, and P. Cluzel. 2004. From molecular noise to behavioural variability in a single bacterium. Nature 428:574-578.
43. Korobkova, E. A., T. Emonet, H. Park, and P. Cluzel. 2006. Hidden stochastic nature of a single bacterial motor. Physical review letters 96:058105.
44. van Albada, S. B., S. Tănase‐Nicola, and P. R. ten Wolde. 2009. The switching dynamics of the bacterial flagellar motor. Molecular systems biology 5:316.
45. Park, H., P. Oikonomou, C. C. Guet, and P. Cluzel. 2011. Noise underlies switching behavior of

the bacterial flagellum. Biophysical journal 101:2336-2340.
46. Wang, F., J. Yuan, and H. C. Berg. 2014. Switching dynamics of the bacterial flagellar motor near zero load. Proceedings of the National Academy of Sciences 111:15752-15755.
47. Lemelle, L., J.-F. Palierne, E. Chatre, and C. Place. 2010. Counterclockwise circular motion of bacteria swimming at the air-liquid interface. Journal of bacteriology 192:6307-6308.
48. Di Leonardo, R., D. Dell'Arciprete, L. Angelani, and V. Iebba. 2011. Swimming with an image. Phys Rev Lett 106:038101.
49. Morse, M., A. Huang, G. Li, M. R. Maxey, and J. X. Tang. 2013. Molecular adsorption steers bacterial swimming at the air/water interface. Biophysical journal 105:21-28.
50. Xie, L., C. Lu, and X.-L. Wu. 2015. Marine Bacterial Chemoresponse to a Stepwise Chemoattractant Stimulus. Biophysical journal 108:766-774.